Supplemental Document

Biomedical Optics EXPRESS

Aberration measurement and correction on a large field of view in fluorescence microscopy: supplement

T. Furieri,[1,2] D. Ancora,[3] G. Calisesi,[3] S. Morara,[4] A. Bassi,[3] and S. Bonora[1,*]

[1] *National Council of Research of Italy, Institute of Photonics and Nanotechnology, via Trasea 7, 35131, Padova, Italy*
[2] *University of Padova, Department of Information Engineering, Via Gradenigo 6, 35131, Padova, Italy*
[3] *Politecnico di Milano, Department of Physics, Piazza Leonardo da Vinci 32, 20133 Milan, Italy*
[4] *National Council of Research of Italy, Institute of Neuroscience, via Vanvitelli 32, 20129, Milan, Italy*
[*] *stefano.bonora@pd.ifn.cnr.it*

Supplement DOI: https://doi.org/10.6084/m9.figshare.16965265

Parent Article DOI: https://doi.org/10.1364/BOE.441810

Aberration measurement and correction on a large field of view in fluorescence microscopy

T. FURIERI,[1,2] D. ANCORA,[3] G. CALISESI,[3] S. MORARA,[4] A. BASSI,[3] S. BONORA[1,*]
1National Council of Research of Italy, Institute of Photonics and Nanotechnology, via Trasea 7, 35131, Padova, Italy
2University of Padova, Department of Information Engineering, Via Gradenigo 6, 35131, Padova, Italy
3Politecnico di Milano, Department of Physics, piazza Leonardo da Vinci 32, 20133 Milan, Italy
4National Council of Research of Italy, Institute of Neuroscience, via Vanvitelli 32, 20129, Milan, Italy

*Corresponding author: stefano.bonora@pd.ifn.cnr.it

SUPPLEMENTARY INFORMATION

Section 1: Performances of the Multi Actuator adaptive Lens

In these experiments we used adaptive lenses, with 10mm clear aperture. The lens is able to generate aberrations up to the 4th order of Zernike polynomials with values reported in Table 4. The optical transmission of the lens is >92% between 400 nm and 1200 nm.

Supplementary Table 1: amount of Zernike polynomials generated by the adaptive lens with 10mm clear aperture.

Aberration	Zernike order	PtV(µm)
Tilt	Z11, Z1-1	16
Defocus	Z20	5.5
Astigmatism	Z22, Z2-2	9.5
Coma	Z31, Z3-1	2.5
Trefoil	Z33, Z3-3	3.8
Spherical Ab.	Z40	0.5
Secondary Ast.	Z42, Z4-2	0.8
Quadrifoil	Z44	1.9

adaptive optics applications. We used a sample target and pocked one actuator at a time for both lenses. Considering k zones inside the field, l lenses with n actuators ($a_{1_1} \dots a_{n_1}, \cdots, a_{1_l} \dots a_{n_l}$), and m pupil sampling points, we sequentially fill the columns of the poke matrix (or influence matrix) that is a $2km$ by n matrix denoted as $\overline{\overline{P}}$.

We can consider it as a block matrix where each block $\overline{\overline{P}}_{ij}$ is the poke matrix of the j_{th} deformable lens acting on the i_{th} field.

$$\overline{\overline{P}} = \begin{pmatrix} \overline{\overline{P}}_{11} & \cdots & \overline{\overline{P}}_{1l} \\ \vdots & \ddots & \vdots \\ \overline{\overline{P}}_{m1} & \cdots & \overline{\overline{P}}_{ml} \end{pmatrix}$$

Finally, we compute the command matrix $\overline{\overline{C}}$ that is a n by $2km$ matrix going from gradient space to actuators space pseudo inverting the poke matrix. This matrix multiplied by the measured wavefront gradients returns the actuator coefficients that can reproduce the gradients with the minimum error. So, the best achievable correction is given by:

$$\overline{c} = -\overline{\overline{C}}\,\overline{w}$$

Where $\overline{w}$ is the measured gradient vector, $\overline{\overline{C}}$ is the command matrix and $\overline{c}$ are the actuators commands.

Section 2: Deconvolution and hardware correction

In first instance, we analyzed the relationship of the deconvolved images with respect to the images SNR. The simulations were carried out starting from experimentally acquired images free of aberrations (mouse kidney sample). See Supplementary Fig. 1.
Each image was convolved with a PSF generated by an increasing amount of spherical aberration and random noise was added to the image to mimic an experimental image acquisition procedure. As expected, the results show that the deconvolution gives better results for the smaller amount of aberration. The Euclidean distances of the images also show that the effect increases more than linearly with the amount of aberration (Fig. 3l). In practice, the stronger the aberration, the less effective is the deconvolution procedure.

To evaluate the effectiveness of the pre-compensation with the deformable lens (see Supplementary Fig. 2), we carried out a different test on the same sample, by including a phase plate that determines a measurable aberration (Blurring PSF) and which we aim to correct. The ground truth image (GT) and the aberrated image (AA) are reported in Supp. Fig. 4a and 4c. By correcting the AA with the software correction (SC) (Richardson-Lucy, 10 steps), we obtain a higher contrast image, shown in Supp. Fig. 4e, but limited resolution. The hardware correction (HC, show in Supp. Fig. 4f), instead, achieves a result that is closer to the real image and with better resolution compared to AA and SC. By plotting the Euclidean distance of the reconstructions against the ground truth, let us quantify the better result obtained by the HC. This study clearly suggests that the hardware correction leads to better results than computational correction because it is not sensitive to SNR variations as it is the case with the deconvolution.

Section 3: Quantification of the distortion
The anisoplanatic deconvolution permits the recovery of an image by mapping the PSF distribution over the image plane. Since the PSF is not uniform in the entire field of view, the result of an anisoplanatic deconvolution differs from that of the isoplanatic one. To quantify the difference between the two reconstructions, we show the absolute distance between the original (blurred) image and the result of the isoplanatic deconvolution (Supplementary Fig. 3, panel a). This helps us to visualize a uniform action of the deconvolution through the entire field of view. In panel b, instead, we display the absolute distance of the isoplanatic versus the anisoplanatic deconvolution. The reconstructions in the central region exhibit a low distance, because the underlined PSF is approximately the same. Instead, the resolution gain is evident in the peripherical regions, where the difference increases radially away from the center as the coma aberration starts to become relevant. The non-uniformity of the PSF introduces an amount of distortion in the recorded image. Here we describe how intensity in the reconstructed image is transported from the isoplanatic to the anisoplanatic reconstruction: we compute the intensity flow by using the Lucas-Kanade method over a window of 5 pixels for the entire field of view, representing the flow as arrows superimposed to the image in panel a. We notice a radial directionality of the deformation, almost negligible in the central patch. In panel c, we report the histogram distribution of its deformation module. We found, on average, a deformation of 0.4μm over the entire image, whereas in the top left tile its mean value increases up to 1.0 μm.

Section 4: Comparison between isoplanatic and anisoplanatic deconvolution

The isoplanatic deconvolution is carried out using the Lucy Richardson method, with the PSF relative to the center of the field of view. For fair comparison with the anisoplanatic deconvolution the used number of iterations is the same in both cases (50). The comparison between the two methods is shown in Supplementary Fig. 4. Both deconvolutions provide similar results in the center, consisting in a small contrast improvement from the hardware corrected case. At the corner of the image the isoplanatic deconvolution is unable to restore a high-quality image.

Section 5: Pupil Plane accuracy

As stated in the paper at section 2.1, the AL location is near enough to the Exit Pupil plane so that we do not see any significant impact on the measurement and correction process. To check for this statement, we measured the aberration due to the couvette only and compared to a simple ray tracing model simulating the condition of the couvette that we have in our microscope. The simulation and the measurement agreed totally showing a spherical aberration component common to all fields and an increasing radial coma the more we moved from the central portion of the FOV. This can be clearly seen in Figure 4 where after the pupil spherical aberration correction, only the residual coma is shown.

Moreover, the results were confirmed by the Adaptive lens calibration process, where the influence function of each actuator is identical for every portion of the FOV.

Supplementary figures

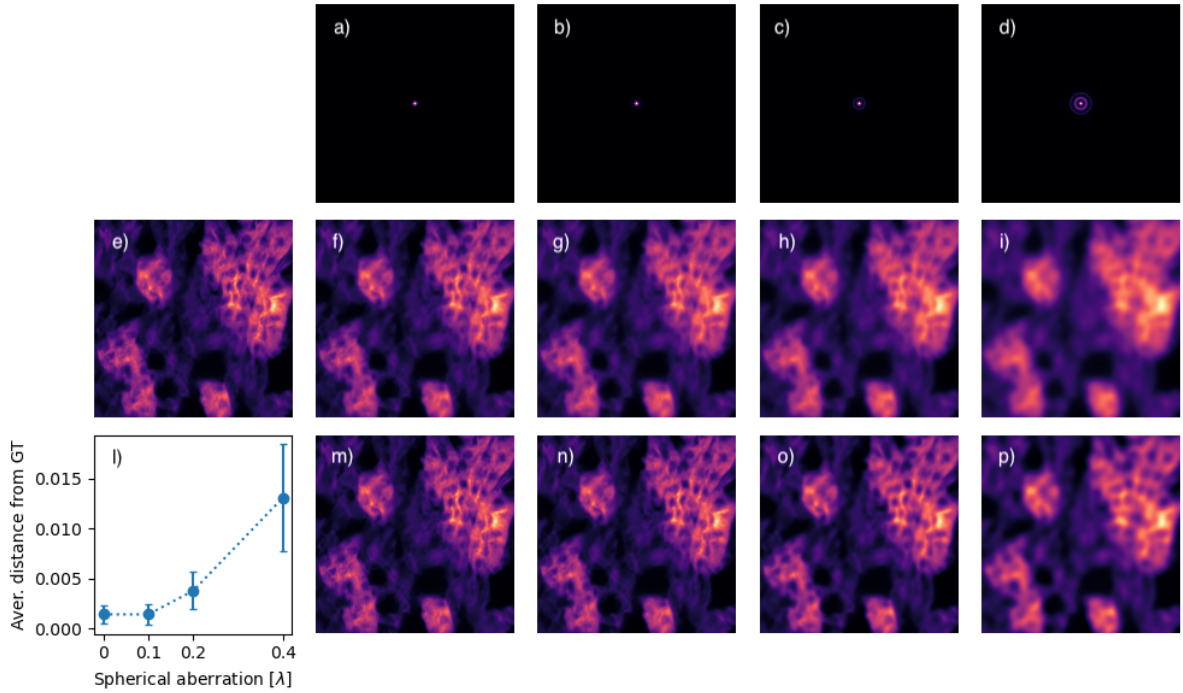

Supplementary Fig. 1: Effect of SNR degradation caused by an increase in the aberration. The ground truth e) has been convolved with different PSF's (a-b-c-d) aberrated with increasing amount of spherical aberration. The resulting images (f-g-h-i) has been deconvolved after adding noise (m-n-o-p). The distance between the ground truth and the deconvolved images is shown in (l).

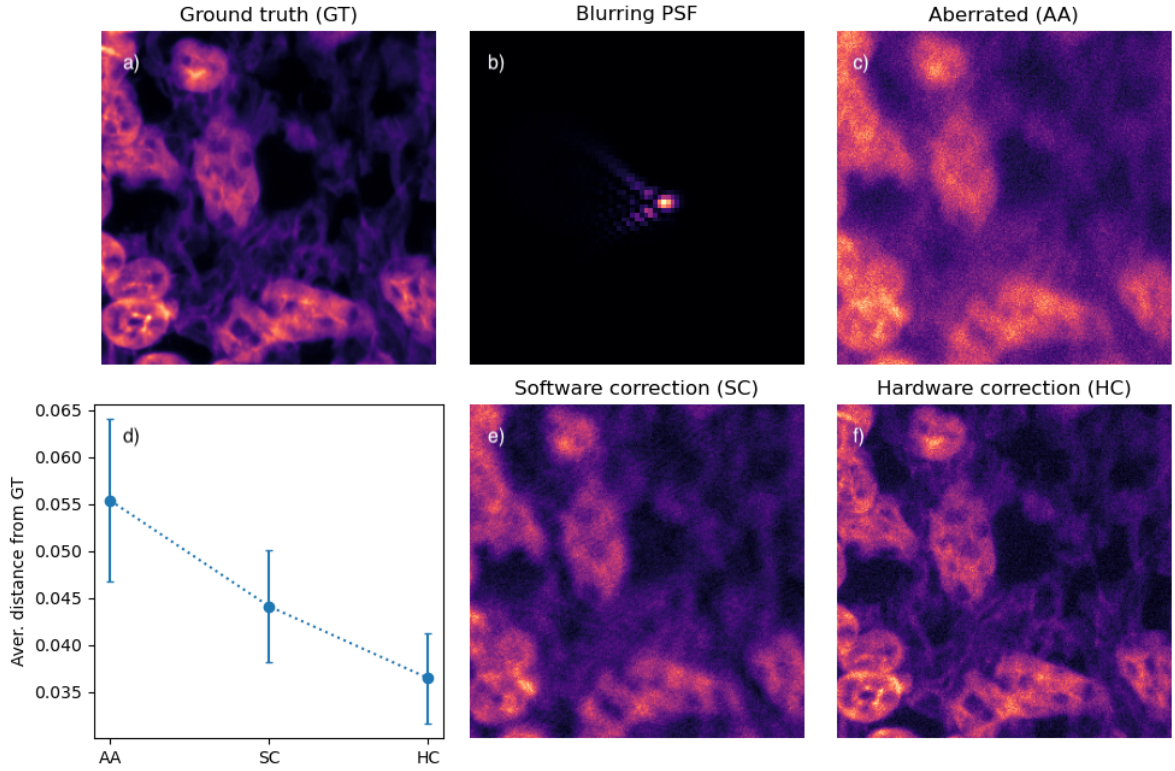

Supplementary Fig. 2: Comparison between hardware and software corrections. The non-aberrated sample, here referred to as the ground truth, (a) has been corrupted by placing an aberrated phase plate in the focusing path which determines a strongly aberrating PSF (b). The phase plate introduces a blurring that results in the aberrated image shown in panel (c). By applying software correction via deconvolution procedure, we obtain the result shown in (e). The hardware correction is

shown in panel (f). We compare the results against the GT in the plot (d) in order to quantify the image quality of the different correction protocols.

Supplementary Fig. 3: (a) Absolute distance between the original image and its isoplanatic deconvolution. The arrows

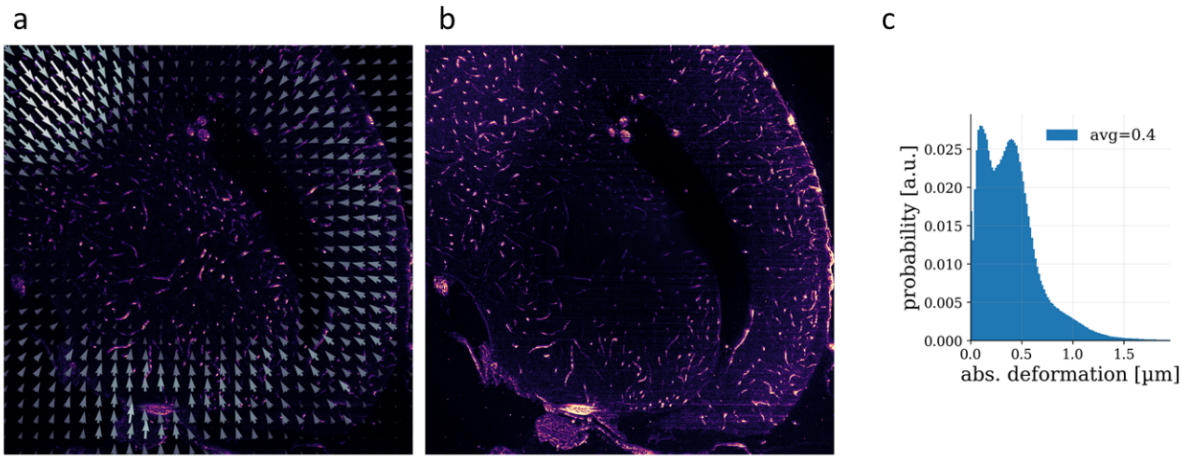

indicate the direction of the deformation of the isoplanatic that are compensated by the anisoplanatic approach. (b) Absolute distance between isoplanatic and anisoplanatic deconvolutions. (c) Histogram of the modulus of the deformation (the arrow length in panel a) over the entire field of view.

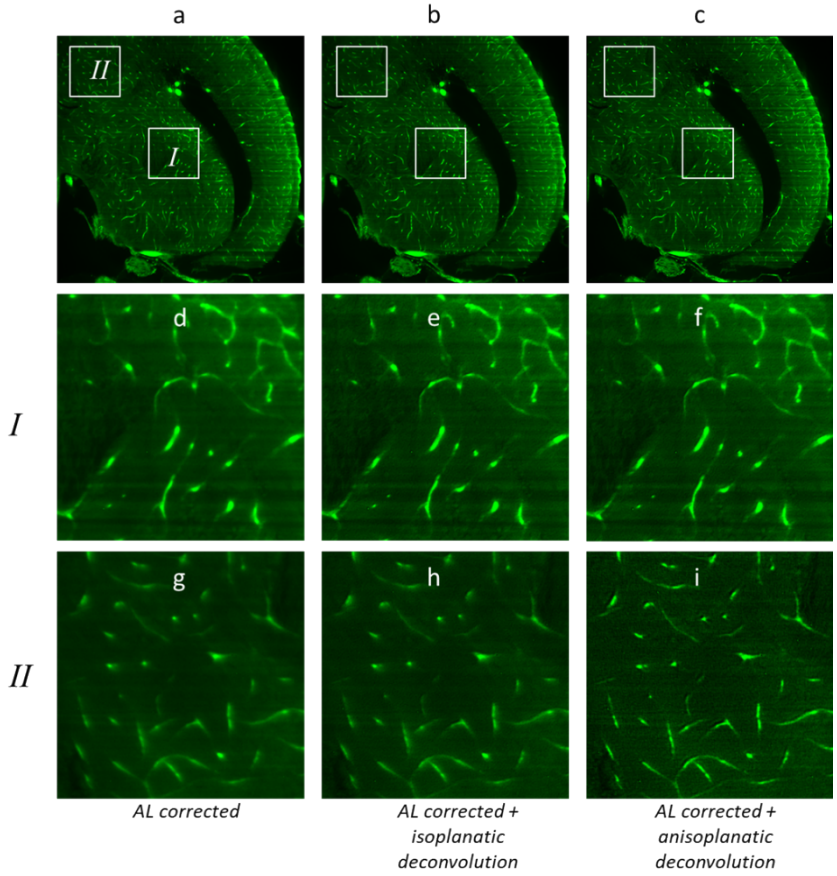

Supplementary Fig. 4: Comparison between (a) hardware correction with adaptive lens AL, (b) combination of hardware correction with isoplanatic deconvolution and (c) anisoplanatic deconvolution. (d-e-f) Magnified region in the center of the field of view. (g-h-i) Magnified region in top right corner.

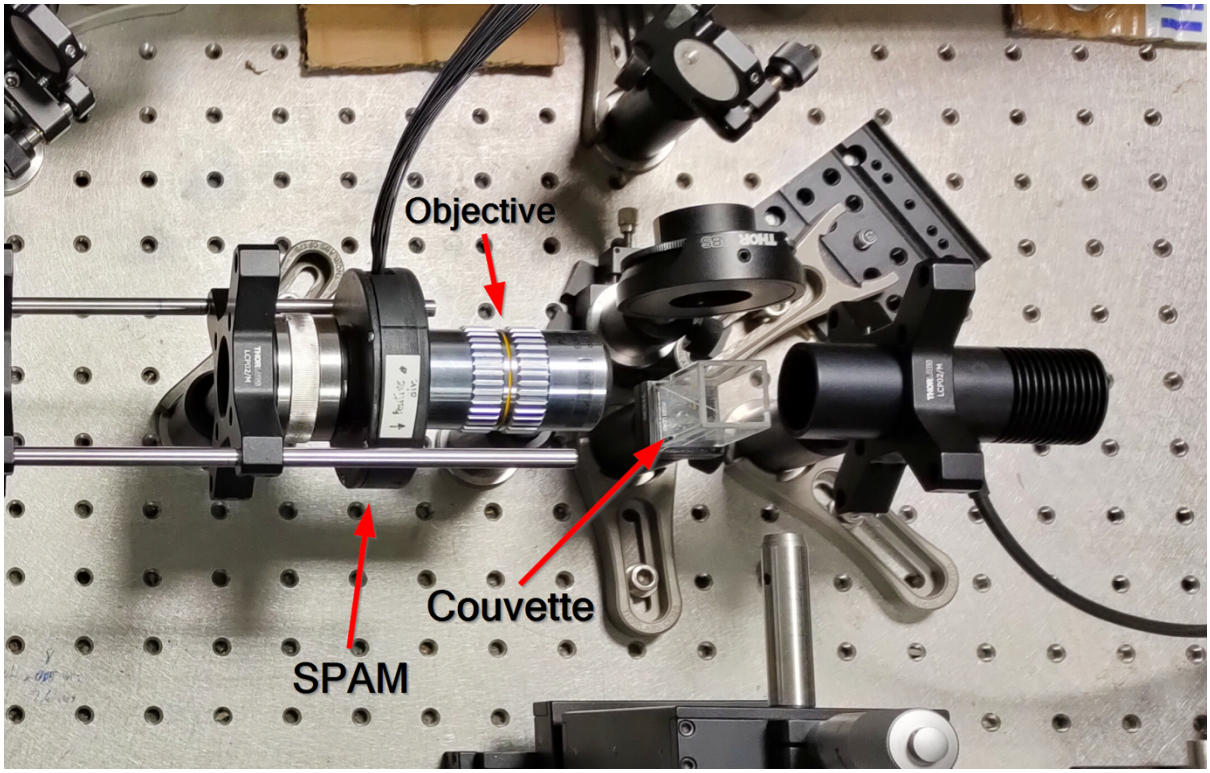

Supplementary Fig. 5: Image of device attached to microscope. The easiness of installation consists in adding only the device screwed to the back aperture of the objective and connecting a multicore cable.